ACS Energy LETTERS

Cite This: ACS Energy Lett. 2019, 4, 2608−2612

http://pubs.acs.org/journal/aelccp

LETTER

Tuning the Closed Pore Structure of Hard Carbons with the Highest Na Storage Capacity

Qingshi Meng, Yaxiang Lu,* Feixiang Ding, Qiangqiang Zhang, Liquan Chen, and Yong-Sheng Hu*

Key Laboratory for Renewable Energy, Beijing Key Laboratory for New Energy Materials and Devices, Beijing National Laboratory for Condensed Matter Physics, Institute of Physics, Chinese Academy of Sciences, Beijing 100190, China

Center of Materials Science and Optoelectronics Engineering, University of Chinese Academy of Sciences, Beijing 100049, China

Supporting Information

ABSTRACT: High-capacity anode materials are one of the bottlenecks to further improve the energy density of Na-ion batteries (NIBs). Except for introducing more defects to increase the sloping capacity, tuning the closed porous structure to boost the plateau capacity is another direction. Here by adopting phenol-formaldehyde resin (PF) as the carbon precursor and ethanol (EtOH) as the pore-forming agent, through precise chemical regulation of their relative content during a solvothermal process before further carbonization, carbon anodes with appropriate microstructure are achieved. It is found that the function of EtOH rests on generating steam vapor to create a pore cavity among cross-linked matrixes. The obtained optimal anodes exhibit a high Na storage capacity of ca. 410 mAh/g. When pairing with an O3-$NaNi_{1/3}Fe_{1/3}Mn_{1/3}O_2$ cathode, the full cell delivers a high initial Coulombic efficiency of 83% and energy density of ca. 300 Wh/kg. The proposed chemical regulation approach via a pore-forming strategy is simple and practical to enable high-energy-density NIBs.

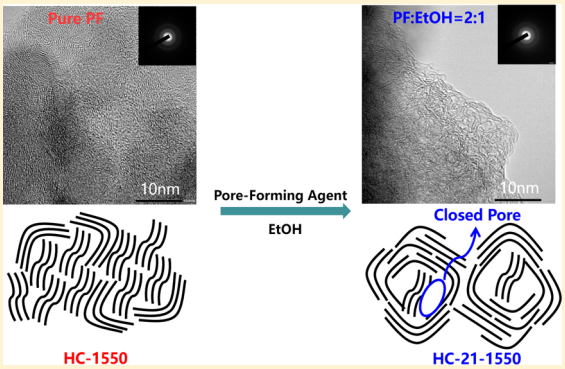

The requirement of sustainable and cost-effective energy storage technology is highly demanded with the increasing awareness of fossil fuel depletion and environmental pollution. Na-ion batteries (NIBs) have recently captured growing interest due to the natural abundance of sodium resources, regarded as a beneficial supplement to Li-ion batteries.[1] Although plenty of cathode materials have been developed, the lack of anode materials with comprehensive good performance impedes further improvement of energy density for NIBs.[2,3] In this respect, the innovation of new strategies to produce affordable and achievable anode materials with remarkable performance is of timely significance.[4−6]

Carbonaceous anodes are very promising for practical use, and massive efforts have been devoted by many research groups.[7−15] In recent years, our group also developed advanced carbon anodes by adopting strategies of hard and soft combination, preoxidation, high/low-temperature treatment, etc.,[16−19] during which the understanding of the Na storage mechanism constantly deepened, where the sloping and plateau capacity relates to surface defects and internal closed pores, respectively. It is no doubt that the plateau capacity is the main contributor to the total capacity of carbon anodes; thus, closed pores are the main microstructure responsible for sodium storage. Therefore, a simple pore-forming strategy to help generate a suitable closed porous structure is crucial to realize high-capacity carbon anodes.

Different from the complicated template[20,21] or self-assembly methods,[22−25] here we propose a green chemical regulation approach via a pore-forming strategy to tune the microstructure evolution. Specifically, the low-cost and producible phenol-formaldehyde resin (PF) is directly used as a carbon precursor, and ethanol (EtOH) acts as the pore-forming agent. After fully mixing and incubating for ∼2h, the mixture is treated through a solvothermal process, during which PF undergoes solidification while EtOH functions as both a reaction agent to accelerate the solidification process and steam generator to induce a pore cavity among the cross-linkage matrixes. It is found that the regulation of EtOH content is the key to achieve an appropriate microstructure after a further carbonization process as large steam gas may burst to open the pore while a small amount of EtOH may directly solidify with PF and could not produce enough vapor to facilitate the formation of a porous structure. A schematic illustration of the green chemical regulation process is shown in Scheme 1.

The general preparation process of hard carbons (HCs) is shown in Figure S1, and the details are shown in the experimental section of the Supporting Information. The HC

Received: August 29, 2019
Accepted: October 4, 2019
Published: October 4, 2019

DOI: 10.1021/acsenergylett.9b01900
ACS Energy Lett. 2019, 4, 2608−2612

Scheme 1. Illustration of the Typical Synthesis Process of Hard Carbon Using Liquid Phenol-Formaldehyde (PF) Resin as the Precursor and EtOH as the Pore-Forming Agent

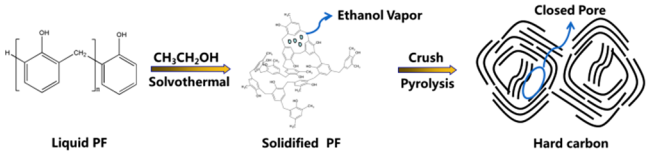

precursors were made from mixture of PF and EtOH with different volume ratios by a solvothermal method (ST), denoted as ST-PF-EtOH-11 (the volume ratio is 1:1), ST-PF-EtOH-21, ST-PF-EtOH-81, and ST-PF. The corresponding HCs prepared at different temperatures were denoted as HC-11-1550, HC-21-1550, HC-81-1550, HC-1550, HC-21-1200, and HC-21-1400. The HC precursors have a smooth surface, and there are tiny holes with a size less than 50 nm (Figure S2). Fourier transform infrared spectroscopy (FTIR) measurements were performed to analyze the effect of EtOH on further polymerization of liquid PF with a low degree of polymerization. As shown in Figure S3, the FTIR spectra of ST-PF are similar to that of ST-PF-EtOH-21. All of the samples contain the stretching vibration of phenolic hydroxyl groups (−OH) at 3500 cm^{-1}, the bending vibration of methylene ($-CH_2-$) at 1465 cm^{-1}, and the stretching vibration of ether groups (C−O−C) at 1125 and 1250 cm^{-1}. The transmittance of the ether groups (C−O−C) of ST-PF-EtOH-21 is obviously lower than that of ST-PF, indicating that EtOH functions as a reaction agent to accelerate the solidification process and has a significant effect on the polymerization and cross-linking degree of PF. After high-temperature pyrolysis, the brown precursor turns into black and exhibits an irregular blocky morphology with a size distribution range of 10−200 μm. In addition, the porous structure could be clearly observed from the surface of the HC-11-1550 sample (Figure S4b).

X-ray diffraction (XRD) and Raman spectroscopy were performed and the results are shown in Figure 1a,b. All XRD patterns have two broad peaks at around 24° and 43°, which can be assigned to the crystallographic planes of (002) and (101) in the disordered carbon structure. With the increasing amount of EtOH, the diffraction pattern remains unchanged, and the (002) diffraction peak has no significant shift, indicating that the average interlayer distance between graphite layers is almost unchanged (Table 1). All of the Raman spectra exhibit two bands: one band at around 1340 cm^{-1} represents the A_{1g} symmetry vibration mode of defects in graphene layer edges (D band), and the other at around 1580 cm^{-1} represents the E_{2g} symmetry vibration mode of an ideal graphitic lattice (G band).[26] The I_D/I_G of HCs calculated from the integrated intensities of the D band and G band shows a bit of decrease when the volume ratio of EtOH is less than 50%, while the I_D/I_G values of HC-21-1550, HC-81-1550, and HC-1550 are close to each other, indicating that the amount of EtOH has little influence on the disordering degree of HCs. The fitting curves of Raman spectra are shown in Figure S5.

High-resolution transmission electron microscopy (HRTEM) and selected area electron diffraction (SAED) were used to investigate the microstructure of the HCs. In general, the sharper diffraction rings of the SAED patterns indicates a more ordered structure in HCs. The disordered and curved graphite sheets are cross-linked to each other, forming

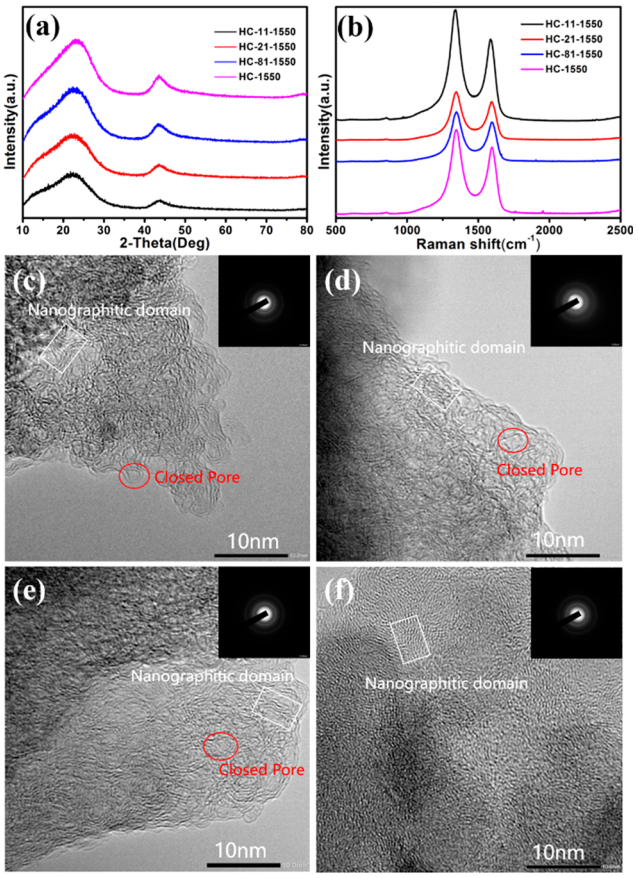

Figure 1. (a) X-ray diffraction patterns and (b) Raman spectrum of HCs prepared by carbonization of a precursor mixed in different amounts of EtOH. Typical HRTEM and SAED images of (c) HC-11-1550, (d) HC-21-1550, (e) HC-81-1550, and (f) HC-1550.

Table 1. Structure Parameters and Electrochemical Properties of HCs

sample	d_{002}[a] (Å)	I_D/I_G[b]	La[c] (nm)	S_{BET} (m^2/g)	RC[d] (mAh/g)	ICE[e] (%)
HC-11-1550	3.94	1.331	14.44	390.84	238	30
HC-21-1550	3.91	1.240	15.50	1.44	384	86
HC-81-1550	3.89	1.245	15.44	0.39	351	82
HC-1550	3.86	1.243	15.46	0.26	304	80

[a] d_{002} is the average interlayer distance. [b] I_D and I_G are the integrated intensities of the D and G bands. [c] La (nm) = $(2.4 \times 10^{-10})\lambda_{nm}^4(I_G/I_D)$. [d] RC is the reversible capacity. [e] ICE is the initial Coulombic efficiency.

closed pores with a diameter less than 2 nm. The local ordered structure constructed by some parallel carbon hexagonal layers can be observed from the turbostratic graphitic microstructures. It is worth noting that both the nanographitic domain and closed pores can be observed in the samples of HC-11-1550, HC-21-1550, and HC-81-1550 (Figure 1c−e). However, the closed pore is hardly visible in the sample of HC-1550 (Figure 1f), indicating that EtOH can induce the formation of a pore cavity among the cross-linkage matrixes of HC.

To figure out the specific surface area and pore size distribution of HCs, the nitrogen adsorption−desorption measurement was performed. The adsorption−desorption isotherms are shown in Figure S6, and the Brunauer−

DOI: 10.1021/acsenergylett.9b01900
ACS Energy Lett. 2019, 4, 2608−2612

Emmett−Teller (BET) surface area is listed in Table 1. The BET surface area is directly related to the amount of EtOH added. With the increasing volume ratio of EtOH, the calculated surface area increases. In the region of high relative pressure, the area enclosed by the adsorption line and the desorption line is larger, indicating that there are a lot of mesopores in HC-11-1550. The HC-11-1550 shows the largest BET surface area of 390.84 m^2/g, much higher than those of HC-21-1550, HC-81-1550, and HC-1550. Such a high specific surface area will lead to the formation of a large amount of solid−electrolyte interface (SEI) films on the surface of HC-11-1550 during the first discharge process, which would reduce the initial Coulombic efficiency. The corresponding electrochemical results are listed in Table 1.

The electrochemical performance of HCs was tested in half-cells with sodium foil as the counter electrode first. Figure 2a

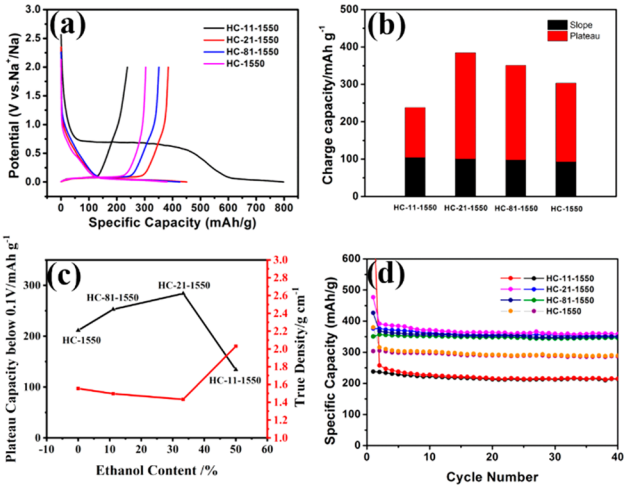

Figure 2. (a) Galvanostatic initial discharge−charge profiles. (b) Specific capacity of HCs contributed from the slope and plateau region. (c) Relationship among the plateau capacity (0.1−0 V), true density, and EtOH content. (d) Cyclic performance of a HC at a current of 0.1C.

displays the initial discharge−charge profiles of the four HC electrodes at a current density of 0.1C (30 mA/g) with a voltage range of 0−2 V. The discharge−charge curves of the samples show typical Na storage behavior of HC materials. The curves can be divided into a high-potential slope region above 0.1 V and a low-potential plateau region below 0.1 V, which correspond to Na ions adsorbed at the defect sites and stored in closed pores, respectively. As shown in Figure 2b, the sloping capacity values of each sample are very similar, manifesting that the amount of added EtOH has little influence on the slope capacity. On the contrary, the plateau capacities of HC-11-1550, HC-21-1550, HC-81-1550, and HC-1550 are 134, 284, 253, and 212 mAh/g, respectively, revealing that the addition of EtOH has a great impact on the plateau capacity. The reasons behind lie in that in the solidification process EtOH acts as a steam generator to induce a pore cavity among the cross-linkage matrixes. The regulation of EtOH content is the key to achieve an appropriate microstructure after a further carbonization process as large steam gas may burst to open the pore while a small amount of EtOH may directly solidify with PF and could not produce enough vapor to facilitate the formation of a porous structure. Therefore, the plateau capacities of HC-21-1550, HC-81-1550, and HC-1550 show a decreased trend.

To further understand how the introduction of EtOH influences the structure of materials, the true density analysis was performed to figure out the effect of EtOH content on closed pores. During the true density test, the volume of open pores and interparticle space can be removed. Therefore, the true density analysis can measure the total volume of closed pores and the solid portion. The true density values decline with the increase of open pores. As shown in Figure 2c, the plateau capacity and true density show an opposite trend with the change of EtOH addition amount, indicating that the number of closed pores increases with the increase of EtOH content, leading to the increase of plateau capacity. The number of closed pores reaches the peak value when EtOH is 33% in the precursor mixture. When the volume content of EtOH reaches 50%, a large number of open pores will be formed, which will rapidly increase the specific surface area and greatly reduce the plateau capacity.

The rate performance was characterized at the current rates from 0.1C to 2C. Due to the low potential in the plateau region, the excessive polarization will significantly reduce the plateau capacity under large current. As shown in Figure S7, the HCs show moderate rate capacity. The cycling performance of HCs was further carried out at a constant current rate of 0.1C, and the results are shown in Figure 2d. The HC-21-1550, HC-81-1550, and HC-1550 samples show capacity retentions of 93, 98, and 94% after 40 cycles, respectively.

To investigate the effect of different carbonization temperatures on the Na storage performance of HCs, HC-21-1200 and HC-21-1400 are prepared. The morphology, structure and relevant parameters of HCs prepared by different carbonization temperatures are shown in Figures S8−S10 and Table S1. The electrochemical performances of HCs with different carbonization temperatures were also tested in half-cells with sodium foil as the counter electrode. Figure 3a shows the initial

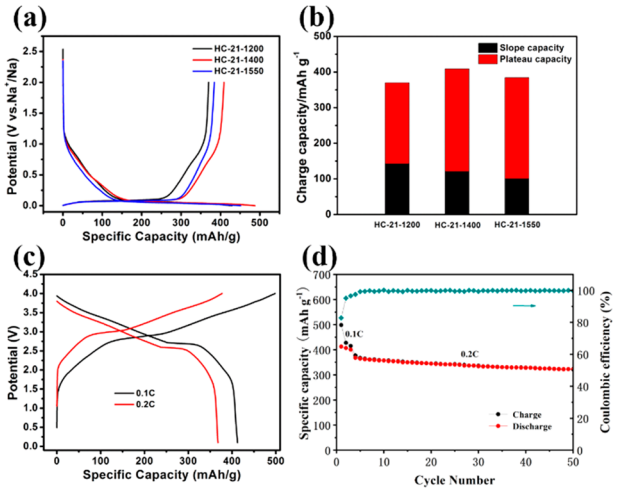

Figure 3. (a) Galvanostatic initial discharge−charge profiles of HC-21-1200, HC-21-1400, and HC-21-1550 samples. (b) Specific capacity of HCs contributed from the slope and plateau regions. Electrochemical performance of the full cell combining O3-$NaNi_{1/3}Fe_{1/3}Mn_{1/3}O_2$ as the cathode material and HC-21-1400 as the anode material. (c) Galvanostatic charge−discharge curves at 0.1C and 0.2C versus specific capacity in the voltage range of 0.1−4.0 V. (d) Cycling performance of the full cell at 0.2C.

DOI: 10.1021/acsenergylett.9b01900
ACS Energy Lett. 2019, 4, 2608−2612

discharge−charge profiles of the three HC electrodes at 0.1C with a voltage range of 0−2 V. As shown in Figure 3b, the reversible capacity of HCs contributed from the slope region decreases obviously with improvement of the pyrolysis temperature, manifesting the reduction of defect sites in HCs. The results are consistent with Raman characterization (Figure S10b). It is worth mentioning that the HC-21-1440 sample exhibits a high reversible capacity of ca. 410 mAh/g and a high initial Coulombic efficiency of 84%, demonstrating the highest capacity among the reported values (Table S2). The rate and cycling performance of HCs with different carbonization temperatures were further carried out, and the results are shown in Figures S11 and S12. The HC-21-1200, HC-21-1400, and HC-21-1550 samples show moderate rate performance from 0.1C to 2C and capacity retentions of 96%, 96%, and 93% after 40 cycles at 0.1C, respectively. The HRTEM image shows that the nanographitic domains and closed pores in HC-21-1400 are basically maintained after cycling, indicating the good cycling stability of the sample (Figure S13).

The coin-type full cell was assembled with O3-Na-$Ni_{1/3}Fe_{1/3}Mn_{1/3}O_2$ as the cathode material and HC-21-1400 as the anode material in order to evaluate the practical application prospect of HCs derived from PF resin. The full cell delivers a high reversible capacity of 413 mAh/g based on the anode mass and 102 mAh/g based on the total mass of the anode and cathode at 0.1C in a voltage range of 0.1−4 V with an average operation voltage of 2.9 V (Figure 3c). The initial Coulombic efficiency can be achieved up to 83%. The energy density of the full cell reaches ca. 300 Wh/kg based on the total mass of the anode and cathode active materials. The cycling performance of the full cell was further carried out at a constant current rate of 0.2C and shows a capacity retention of 87% after 50 cycles (Figure 3d). The outstanding performance of the full cell demonstrates that the HC derived from PF resin is a promising anode material for NIBs.

In summary, we have successfully developed a simple and green chemical regulation strategy to tune the microstructure of PF-derived HC anodes. Through adjusting the content of EtOH, closed pores that have an intimate relationship with the plateau capacity are well controlled. The as-prepared HC-21-1400 shows promising Na storage performance with a high reversible capacity of ca. 410 mAh/g (the plateau capacity accounts for 70%), a high initial Coulombic efficiency of 84%, and a relatively good capacity retention of 96% after 40 cycles. The practical application prospect of synthesized carbon anodes was further demonstrated by an assembled coin-type full cell with O3-$NaNi_{1/3}Fe_{1/3}Mn_{1/3}O_2$ as the cathode material and HC-21-1400 as the anode material. The full cell exhibits a high reversible capacity of 413 mAh/g, a high initial Coulombic efficiency of 83%, and a high energy density of ca. 300 Wh/kg at 0.1C rate. These findings enrich the regulation strategy in microstructure tuning and open new opportunities to design high-performance carbon anodes for NIBs.

■ ASSOCIATED CONTENT

Supporting Information

The Supporting Information is available free of charge on the ACS Publications website at DOI: 10.1021/acsenergylett.9b01900.

Detailed methods for hard carbon preparation; materials characterizations; electrochemical measurements; relative structural and electrochemical characterization results, including Table S1 and Figure S1−S10 (PDF)

■ AUTHOR INFORMATION

Corresponding Authors

*E-mail: yxlu@iphy.ac.cn.
*E-mail: yshu@iphy.ac.cn.

ORCID

Yaxiang Lu: 0000-0001-5202-175X
Yong-Sheng Hu: 0000-0002-8430-6474

Notes

The authors declare no competing financial interest.

■ ACKNOWLEDGMENTS

This work was supported by the National Key Technologies R&D Program of China (2016YFB0901500), the National Natural Science Foundation (NSFC) of China (51725206 and 51421002), NSFC-UKRI_EPSRC (51861165201), the Strategic Priority Research Program of the Chinese Academy of Sciences (XDA21070500), Beijing Municipal Science and Technology Commission (Z181100004718008), Beijing Natural Science Fund-Haidian Original Innovation Joint Fund (L182056), and the Royal Society via the Newton Fund for an Advanced Newton Fellowship.

■ REFERENCES

(1) Kim, H.; Kim, H.; Ding, Z.; Lee, M. H.; Lim, K.; Yoon, G.; Kang, K. Recent Progress in Electrode Materials for Sodium-Ion Batteries. *Adv. Energy Mater.* **2016**, *6* (19), 1600943.

(2) Wang, Q.; Zhao, C.; Lu, Y.; Li, Y.; Zheng, Y.; Qi, Y.; Rong, X.; Jiang, L.; Qi, X.; Shao, Y.; Pan, D.; Li, B.; Hu, Y.-S.; Chen, L. Advanced Nanostructured Anode Materials for Sodium-Ion Batteries. *Small* **2017**, *13* (42), 1701835.

(3) Huang, Y.; Zheng, Y.; Li, X.; Adams, F.; Luo, W.; Huang, Y.; Hu, L. Electrode Materials of Sodium-Ion Batteries toward Practical Application. *ACS Energy Lett.* **2018**, *3* (7), 1604−1612.

(4) Hwang, J.-Y.; Du, H.-L.; Yun, B.-N.; Jeong, M.-G.; Kim, J.-S.; Kim, H.; Jung, H.-G.; Sun, Y.-K. Carbon-Free TiO2Microspheres as Anode Materials for Sodium Ion Batteries. *ACS Energy Lett.* **2019**, *4* (2), 494−501.

(5) Ni, J.; Li, L.; Lu, J. Phosphorus: An Anode of Choice for Sodium-Ion Batteries. *ACS Energy Lett.* **2018**, *3* (5), 1137−1144.

(6) Park, S. K.; Kwon, S. H.; Lee, S. G.; Choi, M. S.; Suh, D. H.; Nakhanivej, P.; Lee, H.; Park, H. S. Cyclable Pseudocapacitive Na-Ion Storage of Hierarchically Structured Phosphorus-Incorporating Nanoporous Carbons in Organic Electrolytes. *ACS Energy Lett.* **2018**, *3*, 724−732.

(7) Jin, J.; Yu, B.-j.; Shi, Z.-q.; Wang, C.-y.; Chong, C.-b. Lignin-based electrospun carbon nanofibrous webs as free-standing and binder-free electrodes for sodium ion batteries. *J. Power Sources* **2014**, *272*, 800−807.

(8) Cao, B.; Liu, H.; Xu, B.; Lei, Y.; Chen, X.; Song, H. Mesoporous soft carbon as an anode material for sodium ion batteries with superior rate and cycling performance. *J. Mater. Chem. A* **2016**, *4* (17), 6472−6478.

(9) Dou, X.; Hasa, I.; Saurel, D.; Jauregui, M.; Buchholz, D.; Rojo, T.; Passerini, S. Impact of the Acid Treatment on Lignocellulosic Biomass Hard Carbon for Sodium-Ion Battery Anodes. *ChemSusChem* **2018**, *11* (18), 3276−3285.

(10) Yamamoto, H.; Muratsubaki, S.; Kubota, K.; Fukunishi, M.; Watanabe, H.; Kim, J.; Komaba, S. Synthesizing higher-capacity hard-carbons from cellulose for Na- and K-ion batteries. *J. Mater. Chem. A* **2018**, *6* (35), 16844−16848.

DOI: 10.1021/acsenergylett.9b01900
ACS Energy Lett. 2019, 4, 2608−2612

(11) Jiang, Q.; Zhang, Z.; Yin, S.; Guo, Z.; Wang, S.; Feng, C. Biomass carbon micro/nano-structures derived from ramie fibers and corncobs as anode materials for lithium-ion and sodium-ion batteries. *Appl. Surf. Sci.* **2016**, *379*, 73−82.
(12) Qian, J.; Wu, F.; Ye, Y.; Zhang, M.; Huang, Y.; Xing, Y.; Qu, W.; Li, L.; Chen, R. Boosting Fast Sodium Storage of a Large-Scalable Carbon Anode with an Ultralong Cycle Life. *Adv. Energy Mater.* **2018**, *8* (16), 1703159.
(13) Li, Q.; Zhu, Y.; Zhao, P.; Yuan, C.; Chen, M.; Wang, C. Commercial activated carbon as a novel precursor of the amorphous carbon for high-performance sodium-ion batteries anode. *Carbon* **2018**, *129*, 85−94.
(14) Li, Z.; Ma, L.; Surta, T. W.; Bommier, C.; Jian, Z.; Xing, Z.; Stickle, W. F.; Dolgos, M.; Amine, K.; Lu, J.; Wu, T.; Ji, X. High Capacity of Hard Carbon Anode in Na-Ion Batteries Unlocked by POx Doping. *ACS Energy Lett.* **2016**, *1* (2), 395−401.
(15) Anji Reddy, M.; Helen, M.; Groß, A.; Fichtner, M.; Euchner, H. Insight into Sodium Insertion and the Storage Mechanism in Hard Carbon. *ACS Energy Lett.* **2018**, *3*, 2851−2857.
(16) Liu, P.; Li, Y.; Hu, Y.-S.; Li, H.; Chen, L.; Huang, X. A waste biomass derived hard carbon as a high-performance anode material for sodium-ion batteries. *J. Mater. Chem. A* **2016**, *4* (34), 13046−13052.
(17) Li, Y.; Hu, Y.-S.; Titirici, M.-M.; Chen, L.; Huang, X. Hard Carbon Microtubes Made from Renewable Cotton as High-Performance Anode Material for Sodium-Ion Batteries. *Adv. Energy Mater.* **2016**, *6* (18), 1600659.
(18) Lu, Y.; Zhao, C.; Qi, X.; Qi, Y.; Li, H.; Huang, X.; Chen, L.; Hu, Y.-S. Pre-Oxidation-Tuned Microstructures of Carbon Anodes Derived from Pitch for Enhancing Na Storage Performance. *Adv. Energy Mater.* **2018**, *8* (27), 1800108.
(19) Qi, Y.; Lu, Y.; Ding, F.; Zhang, Q.; Li, H.; Huang, X.; Chen, L.; Hu, Y. S. Slope-Dominated Carbon Anode with High Specific Capacity and Superior Rate Capability for High Safety Na-Ion Batteries. *Angew. Chem., Int. Ed.* **2019**, *58* (13), 4361−4365.
(20) Lu, P.; Sun, Y.; Xiang, H.; Liang, X.; Yu, Y. 3D Amorphous Carbon with Controlled Porous and Disordered Structures as a High-Rate Anode Material for Sodium-Ion Batteries. *Adv. Energy Mater.* **2018**, *8* (8), 1702434.
(21) Adelhelm, P.; Hu, Y. S.; Chuenchom, L.; Antonietti, M.; Smarsly, B. M.; Maier, J. Generation of Hierarchical Meso- and Macroporous Carbon from Mesophase Pitch by Spinodal Decomposition using Polymer Templates. *Adv. Mater.* **2007**, *19* (22), 4012−4017.
(22) Bin, D.-S.; Li, Y.; Sun, Y.-G.; Duan, S.-Y.; Lu, Y.; Ma, J.; Cao, A.-M.; Hu, Y.-S.; Wan, L.-J. Structural Engineering of Multishelled Hollow Carbon Nanostructures for High-Performance Na-Ion Battery Anode. *Adv. Energy Mater.* **2018**, *8* (26), 1800855.
(23) Jin, Y.; Sun, S.; Ou, M.; Liu, Y.; Fan, C.; Sun, X.; Peng, J.; Li, Y.; Qiu, Y.; Wei, P.; Deng, Z.; Xu, Y.; Han, J.; Huang, Y. High-Performance Hard Carbon Anode: Tunable Local Structures and Sodium Storage Mechanism. *ACS Appl. Energy Mater.* **2018**, *1* (5), 2295−2305.
(24) Tang, J.; Liu, J.; Li, C.; Li, Y.; Tade, M. O.; Dai, S.; Yamauchi, Y. Synthesis of Nitrogen-Doped Mesoporous Carbon Spheres with Extra-Large Pores through Assembly of Diblock Copolymer Micelles. *Angew. Chem., Int. Ed.* **2014**, *54*, 588−593.
(25) Wang, H.-l.; Shi, Z.-q.; Jin, J.; Chong, C.-b.; Wang, C.-y. Properties and sodium insertion behavior of Phenolic Resin-based hard carbon microspheres obtained by a hydrothermal method. *J. Electroanal. Chem.* **2015**, *755*, 87−91.
(26) Sadezky, A.; Muckenhuber, H.; Grothe, H.; Niessner, R.; Pöschl, U. Raman microspectroscopy of soot and related carbonaceous materials: Spectral analysis and structural information. *Carbon* **2005**, *43* (8), 1731−1742.

DOI: 10.1021/acsenergylett.9b01900
ACS Energy Lett. 2019, 4, 2608−2612